The Cl isotope composition and halogen contents of Apollo-return samples

Anthony Gargano[a,b,1], Zachary Sharp[a,b], Charles Shearer[c], Justin I. Simon[d], Alex Halliday[e], and Wayne Buckley[f]

[a]Earth and Planetary Sciences, University of New Mexico, Albuquerque, NM 87131-0001; [b]Center for Stable Isotopes, University of New Mexico, Albuquerque, NM 87131-0001; [c]Institute of Meteoritics, University of New Mexico, Albuquerque, NM 87131-0001; [d]Center for Isotope Cosmochemistry and Geochronology, Astromaterials Research and Exploration Science Division, The Lyndon B. Johnson Space Center, National Aeronautics and Space Administration, Houston, TX 77058; [e]The Earth Institute, Columbia University, New York, NY 10025; and [f]Jacob–Johnson Space Center Engineering, Technology and Science Contract, The Lyndon B. Johnson Space Center, National Aeronautics and Space Administration, Houston, TX 77058

Edited by Mark Thiemens, University of California San Diego, La Jolla, CA, and approved August 6, 2020 (received for review July 9, 2020)

Lunar mare basalts are depleted in F and Cl by approximately an order of magnitude relative to mid-ocean ridge basalts and contain two Cl-bearing components with elevated isotopic compositions relative to the bulk-Earth value of ∼0‰. The first is a water-soluble chloride constituting 65 ± 10% of total Cl with δ^{37}Cl values averaging 3.0 ± 4.3‰. The second is structurally bound chloride with δ^{37}Cl values averaging 7.3 ± 3.5‰. These high and distinctly different isotopic values are inconsistent with equilibrium fractionation processes and instead suggest early and extensive degassing of an isotopically light vapor. No relationship is observed between F/Cl ratios and δ^{37}Cl values, which suggests that lunar halogen depletion largely resulted from the Moon-forming Giant Impact. The δ^{37}Cl values of apatite are generally higher than the structurally bound Cl, and ubiquitously higher than the calculated bulk δ^{37}Cl values of 4.1 ± 4.0‰. The apatite grains are not representative of the bulk rock, and instead record localized degassing during the final stages of lunar magma ocean (LMO) or later melt crystallization. The large variability in the δ^{37}Cl values of apatite within individual thin sections further supports this conclusion. While urKREEP (primeval KREEP [potassium/rare-earth elements/phosphorus]) has been proposed to be the source of the Moon's high Cl isotope values, the ferroan anorthosites (FANs) have the highest δ^{37}Cl values and have a positive correlation with Cl content, and yet do not contain apatite, nor evidence of a KREEP component. The high δ^{37}Cl values in this lithology are explained by the incorporation of a >30‰ HCl vapor from a highly evolved LMO.

chlorine isotopes | apatite | volatiles | halogens

Over the 50 y since the Apollo missions, chemical and isotopic compositions of lunar materials have revolutionized our collective scientific understanding of planetary materials. A major finding is the recognition that lunar materials are strongly depleted in volatiles relative to Earth and that they exhibit a range of volatile-element stable isotope anomalies (1–16). Studying these isotopic systems allows us to better understand volatile sources and mechanisms by which volatile elements are lost throughout planetary evolution. The chlorine isotope system is of particular interest because the Cl isotope values of the Moon are uniquely high. The high values, and increases in the Cl isotope composition of a planetary body from the nebular baseline (around −5 to −7‰ compared to Earth), are related to the amount of Cl that was lost throughout its accretionary and differentiation history (17, 18).

Lunar materials have extremely elevated δ^{37}Cl values relative to the bulk-Earth value of ∼0‰ (14, 19). Sharp et al. (14) measured the bulk and in situ Cl isotope compositions of a variety of lunar lithologies and observed a range in δ^{37}Cl values from −0.7 to 24.5‰. These authors interpreted these results to suggest that anhydrous degassing of lunar magmas resulted in significant Cl isotope fractionation. Many workers have since focused on in situ measurements of late-crystallizing apatite due to the relative ease of this analysis by ion microprobe methods (i.e., secondary-ion mass spectrometry [SIMS] or NanoSIMS). As a result, bulk-rock Cl isotope measurements are few, with limited comparison to the in situ analyses. The δ^{37}Cl values of lunar apatite have been shown to span a large range from 2.2 up to 81.1‰ (20, 21). Typically, the highest δ^{37}Cl values in lunar apatite are observed within lithologies such as the Mg-suite (22), potassium/rare-earth elements/phosphorus (KREEP)-rich basalts and impact lithologies (10), which have largely been explained in terms of a primeval KREEP (urKREEP) component [residual melt of lunar magma ocean (23)] with a characteristically high δ^{37}Cl value (2, 3). This conclusion was initially supported by trends in bulk-rock rare-earth element (REE) content and average apatite δ^{37}Cl value (2, 3), although this trend is not seen in some lithologies (10, 24).

There are two relevant underlying issues that have not been adequately addressed. The first is that for the limited samples in which both bulk and in situ apatite data are available, the apatite invariably has a higher δ^{37}Cl value. The second is that the range of isotope values in apatite measured within a single thin section can exceed 10‰ (e.g., ref. 2). If the high δ^{37}Cl values of some lunar samples is explained by wide-scale incorporation of a urKREEP component (2, 3), then the variation at the thin-section scale should be minimal. A logical explanation for the

Significance

Chlorine isotopes are a sensitive tracer of degassing throughout planetary evolution that provide evidence for the universal depletion of volatiles in the Moon. We show that much of the chlorine in mare basalts is trapped in water-soluble phases from vapor deposition with low isotope values, with the remaining being isotopically heavy from degassing. We also use halogen concentrations and bulk-Cl isotope values to show that most lunar halogen loss and heavy Cl enrichment occurred during the Giant Impact—resulting in a 10× depletion of halogens relative to the Earth. Last, we conclude that lunar apatite has much higher δ^{37}Cl values compared to the bulk rock, likely explained by localized degassing, making their use as direct probes of planetary-scale processes problematic.

Author contributions: A.G. and Z.S. formulated the research questions; C.S. selected samples and provided important insight into lunar petrology; A.G. conducted chlorine isotope analysis with support and guidance from Z.S.; A.G. and W.B. carried out method development and halogen analysis with support and guidance from J.I.S.; A.H. collaborated on sample requests; and A.G. wrote the manuscript with editorial and research advice from all authors.

The authors declare no competing interest.

This article is a PNAS Direct Submission.

Published under the PNAS license.

[1]To whom correspondence may be addressed. Email: agargano@unm.edu.

This article contains supporting information online at https://www.pnas.org/lookup/suppl/doi:10.1073/pnas.2014503117/-/DCSupplemental.

range of apatite δ^{37}Cl values at a small scale is that local degassing, at least in part, controls the chlorine isotope composition of apatite. Extensive degassing of halogens is seen on Earth in volcanic systems (25, 26) and is expected in lunar basalts as well. This explanation, however, opens the possibility that the chlorine isotope compositions of late-formed apatite may not be representative of the bulk rock, and instead preserve the composition of the last melt following extensive degassing. To test this hypothesis and to also address the mechanisms of planetary halogen loss, we analyzed a suite of lunar lithologies for their bulk Cl isotope compositions and mare basalts for halogen (F, Cl, Br, I) contents.

Results

Halogen Concentrations. Cl concentrations were measured on both water-soluble chloride (WSC) and insoluble or structurally bound chloride (SBC) (Table 1). Concentrations of the other halogens (F, Br, I) were measured only on previously leached samples, such that the water-soluble fraction was removed prior to analysis. Previous halogen measurements of lunar samples show that the water-soluble F fraction is minimal (27) and that the Cl/Br ratios are similar between the water-soluble and structural components (28). We therefore assume that our F analyses are a reasonable approximation for the total F in the rock, and that Cl/Br ratios of the insoluble fraction are similar to that of the bulk rock.

For mare basalts, WSC contents range from 1.9 to 10.0 ppm while SBC contents are more restricted, ranging from 1.1 to 5.8 ppm (Table 1). For all mare samples, 65 ± 10% of total Cl resides in the water-soluble fraction. If the WSC is derived from vapor exsolution and deposition, then a significant fraction of the degassed component appears to be retained in the lunar samples. This large fraction of WSC is consistent with studies of terrestrial igneous rocks in which up to 90% of Cl is lost by degassing (25, 26, 29). The mare basalts also have more variable Br concentrations relative to Cl (Table 1) and overall have distinctly lower Cl/Br ratios compared to mid-ocean ridge basalt (MORB) (30, 31) (*SI Appendix*, Fig. S1). The three anorthosite samples average 9 ppm total Cl with variable, but roughly equal proportions in the SBC and WSC.

The F contents of lunar materials range from 4.7 to 38.1 ppm, with highlands lithologies exhibiting a marked depletion relative to mare basalts (Fig. 1). F contents appear to be in-part related to Ti contents (*SI Appendix*, Fig. S2), with high-Ti basalts being the most F-rich from 20.0 to 38.1 ppm. A best fit to the mare samples is a Cl/F = 0.32 ($R^2 = 0.62$). The bulk Cl/F ratios are higher than the average Cl/F ratios of lunar apatite, consistent with the result that the majority of Cl resides in the water-soluble fraction (Table 1). The Cl/F ratios of the insoluble fraction (rinsed samples) overlap the average Cl/F ratio of lunar apatite, further supporting this conclusion. Last, the F and Cl concentration of lunar samples are depleted by an order of magnitude relative to Earth.

Cl Isotope Values. Chlorine isotope values are reported in per mil notation (‰) relative to standard mean ocean chloride (SMOC) (34). The average δ^{37}Cl value for total Cl in mare basalts (sum of WSC + SBC) is 4.1 ± 4.0‰ ($n = 9$). The structural component averages 7.3 ± 3.5‰ ($n = 17$), while the water-soluble fraction averages 1.8 ± 2.5‰ ($n = 8$) (excluding an anomalous WSC value at 12.6‰, 10017-405) (Fig. 2). There is no statistically significant difference between the δ^{37}Cl values of the structurally bound component for high-Ti basalts (7.3 ± 3.1‰, $n = 8$) and low-Ti basalts (6.9 ± 4.1‰, $n = 8$) [two tailed t test: $t_{(14)} = 0.249$, P value = 0.81]. Fig. 2 clearly indicates that the water-soluble fraction for most of the samples is significantly lower than that of the structurally bound Cl. Excluding WSC in sample 10017-405, the isotopic compositions of the WSC and SBC are distinctly different in mare basalts [two-tailed t test: $t_{(24)} = 4.007$, P value = 0.0006]. The three ferroan anorthosite (FAN) samples have much higher δ^{37}Cl values than the mare basalts of 10.5‰, 30.2‰, and 25.2‰ in the SBC, and 11.4‰, 24.5‰, and 25.7‰ in the WSC in samples 60015, 60025, and 62255, respectively. The three non-FAN highlands samples (two norites

Table 1. Halogen contents and δ^{37}Cl values of lunar materials

		Structural Cl		Water-soluble Cl		Structural halogens				
Sample	Lithology	[Cl], ppm	δ^{37}Cl	[Cl], ppm	δ^{37}Cl	[I], ppb	[Br], ppb	[F], ppm	Fraction WSC	Bulk δ^{37}Cl
12002	Low-Ti	2.25	9.40			42.65	138.47	12.81		
10017-400	High-Ti-K	4.37	12.53			206.12	55.26	37.63		
10017-405	High-Ti-K	3.66	9.23	7.25	12.63	28.94	20.16	38.11	0.66	11.49
10020-255	High-Ti	1.90	8.03	3.34	0.39	16.09	14.67	20.84	0.64	3.16
10044-566	High-Ti	1.63	2.62	3.67	1.60	90.77	56.43	30.78	0.69	1.91
12018-277	Low-Ti	1.93	10.05	3.74	5.03	45.50	29.09	18.80	0.66	6.74
12054-146	Low-Ti	2.05	2.14	9.99	−0.78	31.77	6.45	27.08	0.83	−0.28
12054-150	Low-Ti	5.43	4.29	5.51	0.43	60.74	32.96	31.91	0.50	2.35
12063-343	Low-Ti	1.28	4.19	3.83	0.48	30.27	2.69	21.32	0.75	1.41
14053-305	High-Al	5.80	11.24	5.71	6.11	20.11	14.90	33.49	0.50	8.70
15016-240	Low-Ti	1.12	2.14	1.88	0.84	22.26	12.98	11.12	0.63	1.33
15535-165	Low-Ti	1.52	12.12			27.51	162.36	11.39		
15556-258	Low-Ti	1.83	10.57			38.45	153.85	15.37		
70215-389	High-Ti	1.49	6.42			15.09	6.53	31.83		
70255-56	High-Ti	1.57	7.37			24.13	20.87	24.75		
71135-34	High-Ti	3.08	4.01			554.00	34.39	20.02		
74275-355	High-Ti	1.55	8.28			20.80	10.16	19.92		
76335	Troctolite	1.00	4.07			41.45	9.82	4.66		
77215	Cataclastic Norite	2.76	10.26			42.80	15.84	8.77		
78235	Shocked Norite	1.40	6.67			267.8	11.43	8.07		
60015	Cataclastic Anorthosite	0.52	10.50	1.71	11.37				0.77	11.17
60025	FAN	12.10	30.20	3.60	24.45				0.23	28.88
62255	Anorthosite	4.69	25.21	3.44	25.69				0.42	25.41

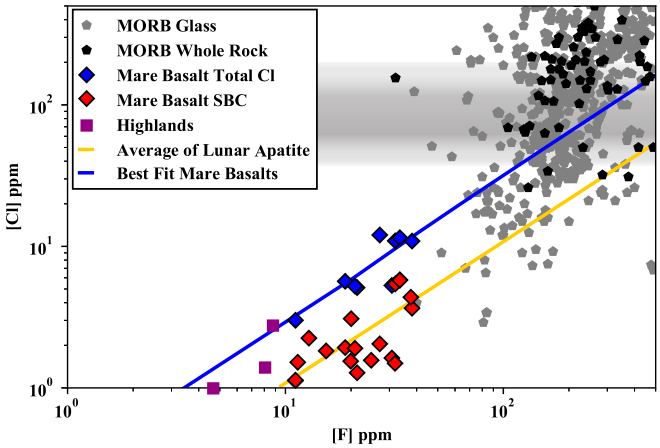

Fig. 1. F vs. Cl contents (ppm) of terrestrial mid-ocean ridge basalts (MORB) (whole rock, black pentagons; glasses, gray pentagons) and lunar materials. The blue diamonds are the total bulk Cl contents of mare basalts (WSC + SBC). The red diamonds are the structurally bound Cl contents. Highlands F and Cl abundances are from the SBC fraction only. Data of MORB collected from the PETDB database. Apatite F and Cl data gathered from refs. 2, 32, and 33 and are seen in the gold line. Blue line represents the best fit for mare basalts. The faded gray horizontal bar is the accepted range of Cl abundances in MORB (30). Higher Cl values are likely contamination. F and Cl errors are smaller than symbol size.

and a troctolite: 76335, 78235, and 77215) have SBC δ^{37}Cl values of 4.07‰, 6.67‰, and 10.3‰, respectively, similar to the mare basalts.

The δ^{37}Cl values of published SIMS analyses of apatite grains from high-Ti and low-Ti mare basalts averages 11.56 ± 4.0‰ (2, 3, 32), a value that is higher and significantly statistically different from the bulk data of 3.2 ± 3.0‰ excluding the WSC of 10017-405 [two-tailed t test: $t_{(78)} = 5.491$, P value = 0.0001], and the structurally bound values of 7.3 ± 3.5‰ [two-tailed t test: $t_{(87)} = 4.075$, P value = 0.0001]. The discrepancy between bulk and in situ δ^{37}Cl values is even more striking for the high-Al and three highlands samples where apatite has δ^{37}Cl values clustering from 20 to 30‰ compared to the SBC average of 8.1‰. Clearly, the δ^{37}Cl values of apatite in these samples are not representative of the bulk rock. Last, no trend is observed between Cl concentration and δ^{37}Cl values [except for FANs (see Fig. 4)], whereas a poor correlation is observed between F contents and bulk total δ^{37}Cl values (*SI Appendix*, Fig. S3).

Discussion

Halogen Degassing. The Cl/F ratios of mare basalts are similar to those of the least altered MORB basalts, but their concentrations are an order of magnitude lower (Fig. 1). As F is thought to be less volatile than Cl, this result suggests that ~90% of halogens were lost during an extremely energetic process, such as the Giant Impact, assuming that the lunar protolith was similar to Earth. Although we anticipated that Cl/Br and Cl/F ratios would correlate with δ^{37}Cl values given the fact that Br is significantly heavier than Cl, and F is less volatile, no trends are observed (*SI Appendix*, Figs. S4 and S5). There is also no apparent relationship in the Cl abundance and δ^{37}Cl values, and only a weak relationship between F abundance and δ^{37}Cl value (*SI Appendix*, Fig. S3), which we interpret as a manifestation of the high δ^{37}Cl values from F-rich apatite grains. Last, Br contents are more variable than Cl, which may be related to differing degrees of retention as the nonsoluble "structurally bound" component. Unfortunately, we were unable to measure water-soluble bromide in any sample as they had already been processed prior to this work, leaving our Br/Cl relationship ambiguous at present.

Chlorine Isotope Composition of Mare Basalts. The majority of Cl in mare basalts is hosted in the water-soluble fraction (Table 1). The water-soluble and structurally bound fractions average 5.0 and 2.5 ppm Cl, respectively. The δ^{37}Cl values of the WSC

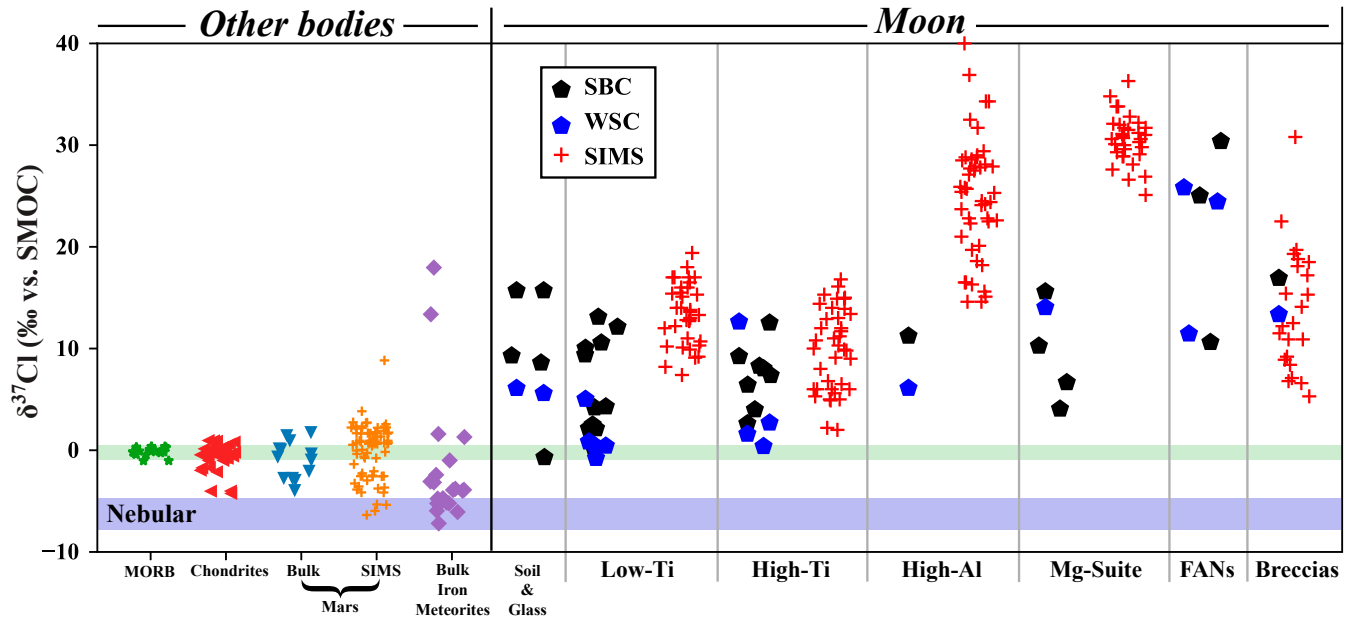

Fig. 2. Chlorine isotope values of planetary and terrestrial materials. MORB data from ref. 19. Bulk lunar data from refs. 14, 15. SIMS data: low-Ti and high-Ti basalts from refs. 3 and 32, high-Al from refs. 2 and 10, highlands from refs. 2 and 35, and breccias from ref. 36. Chondrite data from ref. 19. Martian data from refs. 18 and 37. Iron meteorite data from ref. 17. In-situ lunar apatite δ^{37}Cl values are red crosses. Bulk SBC and WSC δ^{37}Cl values are plotted as black and blue pentagons, respectively. Faded purple bar represents the estimated δ^{37}Cl value of the nebula (17). Faded green bar represents the estimated δ^{37}Cl value of the bulk Earth (19).

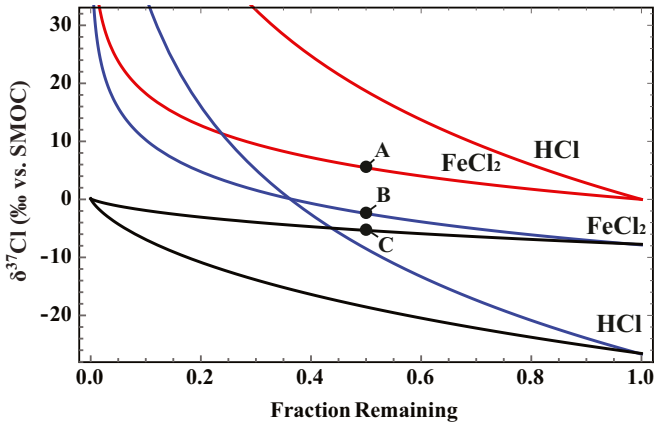

Fig. 3. Rayleigh distillation models of chlorine degassing into a vacuum assuming α values following Graham's Law and Eq. **1**. The red lines show the isotopic composition of the residual fraction (i.e., the degassing reservoir). The blue lines show the instantaneous isotopic composition of vapor derived from the residual melt. The black lines show the isotopic composition of the cumulative vapor component. The isotopic compositions of lunar materials are readily achieved by the degassing of $FeCl_2$ or HCl.

average 1.8 ± 2.5‰ (excluding 10017-405) and are far lower than those of the SBC (7.3 ± 3.5‰) (Fig. 3). Similar differences have been seen in δ^{66}Zn values of water-soluble and structural Zn in Rusty Rock (66095), although the effect is far less pronounced (5), and importantly, the δ^{66}Zn values are anomalously low compared to Earth, while the δ^{37}Cl values are high. If the WSC and SBC were in isotopic equilibrium, we would expect their δ^{37}Cl values to be almost identical, as the fractionation between all chloride-bearing phases is very small at high temperatures (38). Instead, the relatively low isotopically light WSC component is most readily explained by preferential local degassing of ^{35}Cl and subsequent deposition of the light vapor as a water-soluble salt during the waning stages of crystallization. The degassing may occur along fractures or into fluid inclusions and/or vesicles (39). Documentation of visible water-soluble Cl-bearing phases, however, is scarce due to their deliquescent nature and resulting poor preservation. Cl-bearing phases such as akaganéite, lawrencite, and Cl-bearing sulfates have been described in Rusty Rock 66095 (15, 40), and over 60% of Apollo 16 rocks contain a chlorine-bearing "rust" such as akagenéite, which is thought to the be hydrated by-product of $FeCl_2$ (41). Pyroclastic glasses have also been observed to be coated in NaCl (42). In general, the trace amounts of Cl-bearing water-soluble phases have simply not been described in lunar materials due to either a lack of attention or trace deliquescent occurrences being erased by sample preparation/storage procedures.

Arguably the most striking observation in this work is the fact that in no samples measured to date do the bulk δ^{37}Cl values match those of apatite. While the higher Cl/F ratio of the bulk rock compared to lunar apatite supports the observation that significant Cl resides outside of the apatite in the mare basalts (Fig. 1), the poor relationship with δ^{37}Cl values and F contents suggests that other F-bearing phases are also present. As K-rich mesostasis glass is commonly cited in the literature to occur alongside apatite (43), we measured the Cl and F contents of trapped immiscible melts in sample 10050 (low-K, high-Ti basalt) by electron microprobe. Both the K-rich and Fe-rich melts contained significant amounts of F and Cl (1,480, 160, and 5,450, 230 ppm F and Cl, respectively) (*SI Appendix*, Fig. S6). Although no Cl isotope analyses of these Cl-rich glasses have been made, these phases clearly represent another source of Cl and F in lunar materials and partly explain the poor relationship with F contents and δ^{37}Cl values.

In terms of the individual components, lunar apatite has the highest δ^{37}Cl values in mare basalts, averaging 12.6 ± 4.8‰ (high-Ti) and 9.9 ± 4.1‰ (low-Ti). Apatite crystallizes after most of the Cl has been lost to the vapor phase or sequestered in other minerals or glass. The δ^{37}Cl values of the apatite are therefore not representative of the bulk-rock or lunar lithologies in general, but rather record the δ^{37}Cl values of the last stages of crystallization. The loss of a light Cl-bearing vapor raises the δ^{37}Cl value of the residual Cl, which is ultimately incorporated in late-forming apatite and glass. The large spread in δ^{37}Cl values and Cl/F in apatite measured within individual thin sections or even single grains is consistent with apatite forming during the waning stages of crystallization and the final phases of local vaporization.

The overall calculated bulk δ^{37}Cl value of the mare basalts averages 4.1‰, higher than the Earth value, but far lower than the apatite values (Fig. 2). This higher δ^{37}Cl value of the bulk Moon relative to Earth, alongside the poor relationship with F/Cl and δ^{37}Cl values despite the fact the F is less volatile, suggests that lunar halogen depletion and ^{37}Cl enrichment likely resulted from a planet-wide event, presumably the Giant Impact.

Chlorine Isotope Composition of the Highlands Lithologies. The SBC δ^{37}Cl values from troctolite 76335 (4.1‰) and two norites 77215 and 78235 (10.3‰ and 6.7‰) measured are similar to the mare basalts. In contrast, the δ^{37}Cl values of apatite grains from the highlands lithologies (30.6 ± 2.3‰) and the Al-rich basalts (24.9 ± 6.0‰) are far higher than those of the mare basalts (Fig. 2). The low bulk SBC δ^{37}Cl values of highlands troctolites and norites compared to their apatite requires, from mass balance constraints, that the majority of the SBC has a low δ^{37}Cl value and, like the mare basalts, mainly resides somewhere besides the apatite. This conclusion is supported by the fact that the highlands lithologies have far less F, but the same amount of Cl, relative to basalts (*SI Appendix*, Fig. S7). Assuming that the majority of F resides in apatite, then the amount of apatite in these rocks is low compared to the mare basalts. Only the FANs have anomalously high bulk chlorine isotope values, similar to those found in highlands apatite. The δ^{37}Cl values of the SBC and WSC components from the three FANs are similar to each other and exceptionally high (10.5 to 30.2‰) compared to all other lithologies.

It has been suggested that the high δ^{37}Cl values of the highland rocks apatite is due to the incorporation of a high δ^{37}Cl-bearing urKREEP component (2, 3). urKREEP is the hypothetical

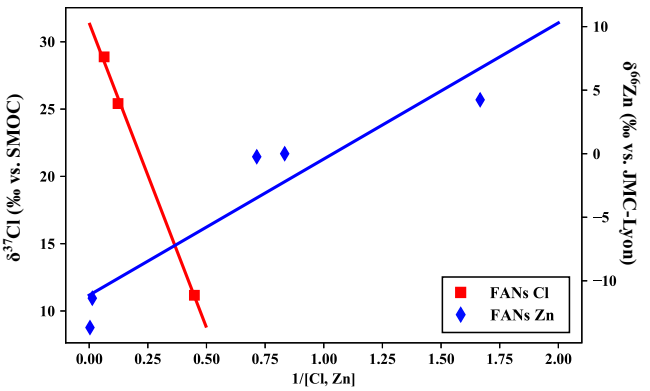

Fig. 4. Plot of 1/[Cl, Zn] (ppm) vs. δ^{37}Cl and δ^{66}Zn value for FANs. The *y* intercept gives the δ^{37}Cl value of the infiltrating gas at 31‰. An initial concentration of 1.5 ppm (before infiltration of Cl vapor) gives a δ^{37}Cl value of pristine FAN of 4‰. Zn data from ref. 7. The red line is the best for the Cl data with an $R^2 = 0.9982$. The blue line is the best fit for the Zn data with an $R^2 = 0.8847$.

reservoir representing the final residue of LMO crystallization (23) and is therefore exceptionally enriched in incompatible trace elements. It has been proposed that urKREEP magma(s) underwent significant degassing and preferentially lost ^{35}Cl to space (3). These high $^{37}Cl/^{35}Cl$ melts were then subsequently incorporated into the highlands lithologies raising their $\delta^{37}Cl$ values. The correlation between the REE abundances and the $\delta^{37}Cl$ values of apatite have been used in support of this argument (2, 3). The causal relationship between urKREEP incorporation and high $\delta^{37}Cl$ values, however, has not been established. One would expect that if the addition of the isotopically heavy and Cl-rich urKREEP occurred, then the Cl content of the rocks would also increase. In other words, in order to raise the $\delta^{37}Cl$ values of the urKREEP-contaminated lithologies, it is necessary to introduce additional heavy Cl. However, the Cl contents of the highlands lithologies are lower, not higher than the mare basalts. Additionally, the FANs are the only lithology to record the high bulk $\delta^{37}Cl$ values characteristic of urKREEP, yet they do not contain apatite, nor do they have clear evidence of a urKREEP component.

An alternative explanation for the high $\delta^{37}Cl$ values of the highland lithologies is their markedly different cooling history compared to mare basalts. The norites, troctolites and anorthosites all cooled very slowly as part of a planet-wide cooling event on the order of 10 °C/Ma (44). In contrast, the mare basalts cooled on the order of ~1 to 20 °C/h (45). The slowly cooled highlands lithologies can therefore be expected to have lost far more Cl during degassing, compared to rapidly cooled mare basalts. Conversely, the high $\delta^{37}Cl$ values of high-Al basalt apatite may also be in-part explained by vapor-phase metasomatism (10). As described below, the effect on the Cl isotope composition of the different rock types can be evaluated using the concept of Rayleigh distillation.

Partial Cl-Retention and Vapor Isotopic Compositions. The isotopic composition of a degassing magma, and the derived vapor can be modeled by use of the Rayleigh distillation equation given by the following:

$$\delta_{\text{Final}} = \delta_{\text{Initial}} + (1{,}000 + \delta_{\text{Initial}}) \times \left(F^{(\alpha-1)} - 1\right), \quad [1]$$

where δ_{Initial} and δ_{Final} are the initial and instantaneous isotopic composition of the melt, F is the fraction of the element remaining and α is the fractionation factor between vapor and melt, given by the following:

$$\alpha_{\text{Vapor-melt}} = \frac{1{,}000 + \delta_{\text{Vapor}}}{1{,}000 + \delta_{\text{Melt}}}. \quad [2]$$

The fractionation α is determined for loss from a melt into a vacuum, governed by Grahams law such that

$$\alpha_{\text{Vapor-melt}} = \sqrt{\frac{M_2}{M_1}}, \quad [3]$$

where M_2 is the molar mass of the volatilizing light isotopologue with ^{35}Cl and M_1 is the molar mass of the heavy isotopologue with ^{37}Cl. For $FeCl_2$, M_2 = 55.8+35.0+35.0 and M_1 = 55.8+35.0+37.0, such that α= 0.992. This is the maximum fractionation for an ideal case where the devolatilizing species passes into a vacuum. The actual fractionation factor will be smaller (α closer to 1). These equations govern how the isotopic composition of instantaneous vapor, the integrated vapor and the residual melt change as degassing proceeds (Fig. 3). Last, the isotopic composition of the cumulative vapor is given by Eq. **4**:

$$\delta_{\text{Cumulative Vapor}} = \frac{\delta_{\text{Initial}} - F(\delta_{\text{Final}})}{1 - F}. \quad [4]$$

When magmatic degassing occurs, the initial vapor has a $\delta^{37}Cl$ value that is $1000ln\alpha$ lower than the magma (−27.8‰ for HCl and −8.0‰ for $FeCl_2$ using α values following Grahams law). The instantaneous $\delta^{37}Cl$ values of the vapor are shown by the blue curves in Fig. 3. The change in the isotopic composition of the residual melt are shown by the red curves. The black curves represent the cumulative $\delta^{37}Cl$ values of the vapor phase as it accumulates, i.e., a case where all vapor is retained in the system. Loss of 50% of the $FeCl_2$ to the vapor phase will raise the residual Cl by ~5.6‰ (point A in Fig. 3). The instantaneous vapor coming off the melt at this point will have a $\delta^{37}Cl$ value ~8.0‰ lighter than the residual (point B). If all Cl vapor that was evolved during degassing was retained in the system, then the total vapor component (equal to the water-soluble chloride) would have a $\delta^{37}Cl$ value of −2.4‰ (point C). In this example, during the earliest stages of degassing, the cumulative vapor component represents a negligible total fraction of Cl. As degassing proceeds, however, the cumulative vapor incorporates an increasing fraction of the total Cl and ultimately approaches the isotopic composition of the initial undegassed melt.

If, instead, the system is open to vapor loss during the early, high-temperature phase of cooling, then different isotope values will be achieved compared to the closed-system case above. This is what we expect for the slowly cooled highlands rocks. During the initial stages of degassing, temperatures would be too high for the vapor phase to condense (5), and the light vapor component would not be retained. Given the extremely slow cooling rates, the vapor would migrate out of the system and be lost from the system with the $\delta^{37}Cl$ value of the rock progressively increasing. Loss of a significant fraction of the light vapor, as expected in the slowly cooled highlands rocks, results in high $^{37}Cl/^{35}Cl$ in the residue, and thus explains the elevated bulk values and the very high $\delta^{37}Cl$ values of their late-formed apatite grains.

Anomalous Cl and Zn Isotope Compositions of FANs. The FANs are thought to represent the primitive lunar crust that formed by the accumulation of buoyant plagioclase over the lunar magma ocean (LMO) (46, 47). Standard LMO crystallization models state that the primitive lunar crust would have formed a thermally insulating "lid" on the crystallizing magma ocean, potentially limiting volatile loss to space (2, 4, 48). However, volatiles would have continually percolated through the crust post-crystallization (41), possibly during a global mode of volcanic "heat-pipes" transporting melt to the surface (49), or be lost by crust-breaching impacts (2). The bulk $\delta^{37}Cl$ values of FANs are the highest measured in planetary materials to date and positively correlate with Cl contents, opposite from what would be expected from a simple open system degassing trend (Fig. 4). Instead, the data suggest incorporation and deposition of a heavy Cl-bearing vapor into the FANs. This is consistent with Cl being incorporated in the FANs only after most had passed through the lithology as a gas phase. Zn isotope compositions on the other hand, have a negative correlation with concentration (7) suggesting that the FANs incorporated an early degassed light Zn-bearing phase.

Exotic sources of Cl and Zn to the FANs such as chondrites or regolith can be discounted on the basis that both Cl and Zn isotope values, as well as elemental concentrations, are a poor match. A heavy urKREEP source could also be invoked to explain the FANs high $\delta^{37}Cl$ values. Some KREEPy lithologies (i.e., Mg-suite) are thought to represent plutonic emplacements into the lunar crust and therefore the proximity of the FANs and urKREEP is certainly feasible. McCubbin et al. (2015) estimates KREEP melts likely contained 1.4 wt% Cl when apatite began to

crystallize which record the characteristically high Cl isotope compositions. Mixing with 0.1% KREEP with a δ^{37}Cl value of +30‰ could explain the highest [Cl] and δ^{37}Cl reported here, however, this mixing component is not seen in elevated REE patterns or any other geochemical system to our knowledge. Additionally, the FANs were likely emplaced prior to urKREEP formation (50), and their Zn isotope compositions are also distinct from KREEPy samples, with comparable [Zn] but with significantly lower δ^{66}Zn values (7). In total, assimilation of urKREEP is inconsistent with both Cl and Zn isotope data (51). We instead propose that the Cl and Zn isotope compositions resulted from vapor deposition from the degassing of underlying magma(s).

While it has generally been assumed that Zn and Cl both degas as chlorides (and ZnS), the isotopic compositions of the FANs require that these two elements are decoupled (see also ref. 5). Assuming that Zn and Cl had similar volatilities, they would vaporize and condense over roughly the same temperature interval. If this were the case, low δ^{66}Zn values would occur alongside low δ^{37}Cl values, which is clearly not seen in the data for the FANs or other samples such as Rusty Rock. Furthermore, it is difficult to explain the very low δ^{66}Zn values of −13.7‰ found in Rusty Rock, or −11.4‰ in 65315 using a simple Rayleigh fractionation model if $ZnCl_2$ is assumed to be the degassing species and the initial δ^{66}Zn value of the source was close to 0‰. This is because the maximum $1000ln\alpha$ value for $ZnCl_2$ is only −7.4‰, far less than the ∼13–14‰ fractionation for Rusty Rock (5). The trends seen in Fig. 4 make coupled degassing equally unlikely for the FANs.

We instead propose that the low δ^{66}Zn values are better explained by the degassing of Zn^o from the underlying magma and subsequent deposition in the FANs at relatively high temperatures, as suggested by recent thermodynamic modeling (52). Importantly, the 1000lnα value of Zn^o degassing is −15.4‰, compared to only −7.4‰ for $ZnCl_2$ (assuming Grahams law applies). In contrast to Zn^o gas, which condenses at around 700 °C, metal chloride species are volatile above 500 °C (52, 53). In the most extreme case where Cl is transported as HCl, Cl would never condense. It would only become incorporated in a rock when it reacts to form a solid chloride phase (e.g., $FeCl_2$). Zn^o gas derived from the underlying magma ocean would degas through the FANs where the high condensation temperatures of ZnS or Zn^o would lead to only a small amount of Zn migrating to the higher and colder levels of the FANs. As the FANs cool, the migration distance of the Zn decreases from the underlying magma, such that only the early, light Zn would be found in the upper level of the FANs, which is presumably what is sampled in the Apollo collection.

Cl differs from Zn because it has a lower condensation temperature. As long as the anorthositic lid remained hot, Cl would not condense, but rather pass through the FANs. Retention of this vapor percolating through the FANs would only have occurred when temperatures dropped sufficiently for Cl-bearing vapors to condense (e.g., ref. 5). If most of the Cl had already been lost from the underlying magma before it could condense in the FANs, then the δ^{37}Cl value of the vapor that was ultimately incorporated would be isotopically heavy (Fig. 5). In the case of HCl degassing, loss of 90% of the total Cl would raise the vapor value to over 30‰. For $FeCl_2$, the amount lost would be closer to 99%. Addition of the heavy vapor would have increased both the Cl concentration and the δ^{37}Cl value, and indeed, a negative linear mixing trend of 1/[Cl] vs. δ^{37}Cl is seen in the limited data for the FANs, supporting this hypothesis (Fig. 4). In total, the partial Cl-retention model in the FANs suggests they were only partially effective in limiting volatile-loss to the surface and future modeling of LMO volatile-loss should account for the continued loss of volatiles after FAN crystallization (54).

Conclusion

There are several important findings in this work. First, the bulk Cl isotope compositions of lunar mare basalts is 3–4‰ higher than the bulk Earth and the halogen concentration of lunar lithologies is an order of magnitude lower than MORB. We propose that these differences are the result of an early planetary-wide halogen depletion and isotope fractionation associated with the Giant Impact, similar to what is seen for other volatile elements (e.g., refs. 9, 55).

Second, we find a large isotope fractionation between the water-soluble and structurally bound chloride within individual samples. Approximately 65% of Cl in the mare basalts is hosted in a water-soluble with an average δ^{37}Cl value of 1.8 ± 2.5‰ (excluding 10017–405). The remaining insoluble or structurally bound chloride averages δ^{37}Cl values of 7.3 ± 3.5‰.The large difference in the isotopic composition of these two coexisting Cl reservoirs cannot be explained in terms of equilibrium, high-temperature isotope fractionation (38). Instead, the low δ^{37}Cl values of the vapor component are explained by kinetic isotope fractionation during local degassing and subsequent deposition. The δ^{37}Cl values of apatite grains are significantly higher than the bulk δ^{37}Cl values in all lithologies. Rather than being representative of the bulk rock, apatite δ^{37}Cl values record information about the final stages of crystallization. Local degassing during late-stage crystallization explains the wide range of δ^{37}Cl values seen in apatite grains within individual thin sections.

Third, the highlands rocks have extremely elevated δ^{37}Cl values in apatite, but only moderately elevated bulk δ^{37}Cl values (Fig. 2). We explain the high δ^{37}Cl values of the late-formed apatite as being a result of the slow cooling rate for these plutonic lithologies resulting in extensive Cl degassing prior to apatite formation. Compared to the mare basalts, cooling of the magma ocean and overlying solid lithologies was many orders of magnitude slower. The very slow cooling would result in a larger fraction of Cl to be lost to the vapor phase, thereby causing the residual melt to have increasingly high δ^{37}Cl values. This effect is especially notable for the late-formed apatite which records the highest δ^{37}Cl values (Fig. 4).

Finally, the FANs uniquely have extremely high δ^{37}Cl values for both the WSC and SBC (Fig. 2), although they have no

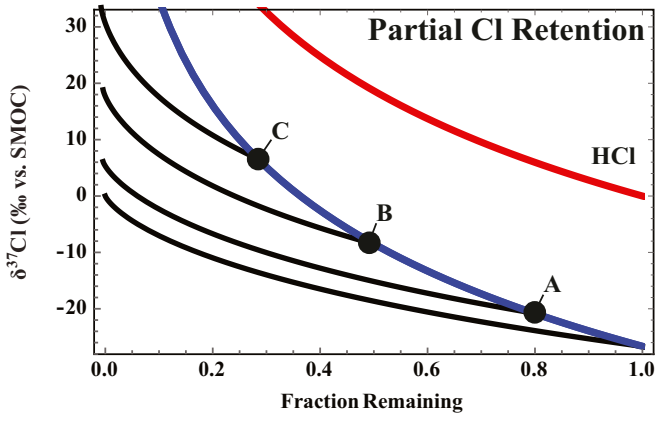

Fig. 5. Modified Rayleigh distillation model showing partial chlorine retention. Line legend is the same as in Fig. 3. In this model, we choose to use HCl as an isotopologue capable of reaching the largest range of δ^{37}Cl values. Three different arbitrary points are chosen for schematic purposes (A, B, and C) in which to vapor derived from an underlying melt is retained. If vapor begins to be retained at point A and is completely incorporated, it will have a δ^{37}Cl value of +6‰ with 80% of initial [Cl]. Likewise, for B with a δ^{37}Cl of +20‰ and 50% of initial [Cl], and last C with a δ^{37}Cl of +34‰ and 30% initial [Cl]. The partial retention of chlorine following this model will show increasing δ^{37}Cl with [Cl].

urKREEP component, nor apatite grains. This result is at odds with the hypothesis that the high δ^{37}Cl values of highlands rocks is related to incorporation of urKREEP. Instead, we suggest that their extremely high δ^{37}Cl values are explained as the product of condensation of a heavy Cl-bearing vapor. The anorthosite layer above the crystallizing magma ocean would have been extremely hot post crystallization. The Cl-bearing vapor derived from the underlying magma would therefore pass through the anorthositic lid without condensing. Only after extensive degassing would the anorthosite layer cool sufficiently for the Cl-bearing vapor to condense. By the time this occurred, the vapor would have evolved to a very high δ^{37}Cl value (>30‰) which is supported in the positive correlation between Cl content and δ^{37}Cl values. In contrast, Zn has a much higher condensation temperature (over 700 °C for ZnS). Only the earliest, and thereby the isotopically lightest Zn^o vapor would penetrate to the upper layers of the FANs resulting in the incorporation of Zn with exceptionally low δ^{66}Zn values. Once the FANs cooled below 700 °C, Zn migration distances would be severely curtailed. The very low δ^{66}Zn values of FANs (and Rusty Rock) are thereby best explained by degassing of Zn^o where the 1000lnα value is significantly higher than for higher mass Zn-bearing compounds.

Materials and Methods

Cl isotope compositions of a suite of lunar materials were measured following the methodology of Sharp et al. (14) at the University of New Mexico. Water-soluble chloride (WSC) was collected by leaching powders with de-ionized water overnight. Structurally bound chloride (SBC) was extracted by pyrohydrolysis on the residual powders following WSC leaching. Leached powders were rinsed an additional 3 times before drying to remove any residual WSC component, dried and then loaded into quartz tubes. Samples were then subsequently pyrolyzed by melting with an oxy-propane torch in a stream of water vapor within a distillation apparatus (2). An aliquot of parent solutions were measured at National Aeronautics and Space Administration (NASA) Johnson Space Center for Cl, Br and I contents by ICPMS following the methodology of ref. 56. Average 1σ deviation on Cl, Br and I contents were 2.2, 11.4, and 1.14%, respectively. Additional information regarding halogen measurements can be found in the *SI Appendix*. Fluorine contents were measured at UNM using Ion Chromatography.

A split of the sample solutions were reacted with 5 mL of 50% HNO_3 overnight in order to remove sulfur, followed by an addition of 1 mL of 0.4 M $AgNO_3$ overnight in a light-free environment in order to precipitate AgCl. AgCl was then filtered, dried, and loaded into 8 mm Pyrex tubes. Sample tubes were then evacuated, 10 μL of CH_3I was added and subsequently flame sealed. Sealed tubes were then reacted at 80 °C for 48 h to produce CH_3Cl as an analyte. Introduction of CH_3Cl into the mass spectrometer took place by cracking sealed sample tubes in a stream of He and collecting the CH_3Cl in a liquid N_2 trap. This trap was subsequently warmed, and the sample gas was passed through a GC column held at 80 °C to separate excess CH_3I from the CH_3Cl analyte. A small "sniffer" capillary was used to detect when CH_3Cl had completely left the column and was trapped in a second liquid N_2 trap. Flow direction was then reversed prior to the incorporation of CH_3I, which resulted in a pure CH_3Cl sample. Trapped CH_3Cl was then released by warming the LN_2 trap and introduced via an open split into the mass spectrometer. Chlorine isotope compositions were measured in continuous flow on a Delta^{PLUS}XL. Measurements were standardized relative to SMOC with a long-term reproducibility of this method being less than ±0.25‰ in our laboratory.

Data Availability. All study data are included in the article and *SI Appendix*.

ACKNOWLEDGMENTS. We thank Curation and Analysis Planning Team for Extraterrestrial Materials and the Astromaterials Acquisition and Curation Office at NASA Johnson Space Center for the allocation of lunar samples and the Astromaterials Research Office for generous access to the Center for Isotope Cosmochemistry and Geochronology Laboratory at NASA Johnson Space Center to develop the method for measuring trace halogen contents in planetary materials. This research was supported by NASA Graduate Fellowship 17-AS&ASTAR17-0026 awarded to A.G. and NASA Planetary Science funding that partially supported his research activities at NASA Johnson Space Center. We also thank two reviewers for helpful comments.

1. J. J. Barnes *et al*., An asteroidal origin for water in the Moon. *Nat. Commun.* **7**, 11684 (2016).
2. J. J. Barnes *et al*., Early degassing of lunar urKREEP by crust-breaching impact(s). *Earth Planet. Sci. Lett.* **447**, 84–94 (2016).
3. J. W. Boyce *et al*., The chlorine isotope fingerprint of the lunar magma ocean. *Sci. Adv.* **1**, e1500380 (2015).
4. J. M. Day, F. Moynier, Evaporative fractionation of volatile stable isotopes and their bearing on the origin of the moon. *Philos. Trans. R. Soc. A* **372**, 26 (2014).
5. J. M. D. Day, F. Moynier, C. K. Shearer, Late-stage magmatic outgassing from a volatile-depleted Moon. *Proc. Natl. Acad. Sci. U.S.A.* **114**, 9547–9551 (2017).
6. C. Kato, F. Moynier, Gallium isotopic evidence for extensive volatile loss from the Moon during its formation. *Sci. Adv.* **3**, e1700571 (2017).
7. C. Kato, F. Moynier, M. C. Valdes, J. K. Dhaliwal, J. M. D. Day, Extensive volatile loss during formation and differentiation of the Moon. *Nat. Commun.* **6**, 7617 (2015).
8. F. Moynier, F. Albarède, G. F. Herzog, Isotopic composition of zinc, copper, and iron in lunar samples. *Geochim. Cosmochim. Acta* **70**, 6103–6117 (2006).
9. R. C. Paniello, J. M. D. Day, F. Moynier, Zinc isotopic evidence for the origin of the Moon. *Nature* **490**, 376–379 (2012).
10. N. J. Potts, J. J. Barnes, R. Tartèse, I. A. Franchi, M. Anand, Chlorine isotopic compositions of apatite in Apollo 14 rocks: Evidence for widespread vapor-phase metasomatism on the lunar nearside ~4 billion years ago. *Geochim. Cosmochim. Acta* **230**, 46–59 (2018).
11. E. A. Pringle, F. Moynier, Rubidium isotopic composition of the Earth, meteorites, and the Moon: Evidence for the origin of volatile loss during planetary accretion. *Earth Planet. Sci. Lett.* **473**, 62–70 (2017).
12. K. L. Robinson *et al*., Water in evolved lunar rocks: Evidence for multiple reservoirs. *Geochim. Cosmochim. Acta* **188**, 244–260 (2016).
13. A. E. Saal, E. H. Hauri, J. A. Van Orman, M. J. Rutherford, Hydrogen isotopes in lunar volcanic glasses and melt inclusions reveal a carbonaceous chondrite heritage. *Science* **340**, 1317–1320 (2013).
14. Z. D. Sharp, C. K. Shearer, K. D. McKeegan, J. D. Barnes, Y. Q. Wang, The chlorine isotope composition of the moon and implications for an anhydrous mantle. *Science* **329**, 1050–1053 (2010).
15. C. K. Shearer *et al*., Chlorine distribution and its isotopic composition in "rusty rock" 66095. Implications for volatile element enrichments of "rusty rock" and lunar soils, origin of "rusty" alteration, and volatile element behavior on the Moon. *Geochim. Cosmochim. Acta* **139**, 411–433 (2014).
16. B. A. Wing, J. Farquhar, Sulfur isotope homogeneity of lunar mare basalts. *Geochim. Cosmochim. Acta* **170**, 266–280 (2015).
17. A. Gargano, Z. Sharp, The chlorine isotope composition of iron meteorites: Evidence for the Cl isotope composition of the solar nebula and implications for extensive devolatilization during planet formation. *Meteorit. Planet. Sci.* **54**, 1619–1631 (2019).
18. J. Williams *et al*., The chlorine isotopic composition of Martian meteorites 1: Chlorine isotope composition of Martian mantle and crustal reservoirs and their interactions. *Meteorit. Planet. Sci.* **51**, 2092–2110 (2016).
19. Z. Sharp *et al*., The chlorine isotope composition of chondrites and Earth. *Geochim. Cosmochim. Acta* **107**, 189–204 (2013).
20. B. L. Jolliff, M. A. Wieczorek, C. K. Shearer, C. R. Neal, *New Views of the Moon*, (Walter de Gruyter, 2018), Vol. vol. 60.
21. Y. Wang, W. Hsu, Y. Guan, An extremely heavy chlorine reservoir in the Moon: Insights from the apatite in lunar meteorites. *Sci. Rep.* **9**, 5727 (2019).
22. F. McCubbin, J. Barnes, "Chlorine-isotopic analysis of apatite in an olivine-hosted melt inclusion in magnesian-suite troctolite 76535: Further evidence of a KREEP-rich parental magma?" in *Lunar and Planetary Science Conference Proceedings 51*, (Lunar and Planetary Institute, Houston, TX, 2020), p. 2415.
23. P. H. Warren, J. T. Wasson, The origin of KREEP. *Rev. Geophys.* **17**, 73–88 (1979).
24. A. H. Treiman *et al*., Phosphate-halogen metasomatism of lunar granulite 79215: Impact-induced fractionation of volatiles and incompatible elements. *Am. Mineral.* **99**, 1860–1870 (2014).
25. D. C. Noble, V. C. Smith, L. C. Peck, Loss of halogens from crystallized and glassy silicic volcanic rocks. *Geochim. Cosmochim. Acta* **31**, 215–223 (1967).
26. H. Balcone-Boissard, B. Villemant, G. Boudon, Behavior of halogens during the degassing of felsic magmas. *Geochem. Geophys. Geosyst.* **11**, 9 (2010).
27. G. W. Reed, S. Jovanovic, Fluorine in lunar samples: Implications concerning lunar fluorapatite. *Geochim. Cosmochim. Acta* **37**, 1457–1462 (1973).
28. G. W. J. Reed, S. Jovanovic, "Halogens, mercury, lithium and osmium in Apollo 11 samples" in *Proceedings of the Apollo 11 Lunar Science Conference 2*, A. A. Levinson, Ed. (Pergamon, New York, 1970), pp. 1487–1492.
29. L.-X. Wang, M. A. Marks, J. Keller, G. Markl, Halogen variations in alkaline rocks from the Upper Rhine Graben (SW Germany): Insights into F, Cl and Br behavior during magmatic processes. *Chem. Geol.* **380**, 133–144 (2014).
30. A. Jambon, B. Déruelle, G. Dreibus, F. Pineau, Chlorine and bromine abundance in MORB: The contrasting behaviour of the mid-Atlantic ridge and East Pacific Rise and implications for chlorine geodynamic cycle. *Chem. Geol.* **126**, 101–117 (1995).
31. M. A. Kendrick, V. S. Kamenetsky, D. Phillips, M. Honda, Halogen systematics (Cl, Br, I) in mid-ocean ridge basalts: A Macquarie Island case study. *Geochim. Cosmochim. Acta* **81**, 82–93 (2012).
32. J. J. Barnes, I. A. Franchi, F. M. McCubbin, M. Anand, Multiple reservoirs of volatiles in the Moon revealed by the isotopic composition of chlorine in lunar basalts. *Geochim. Cosmochim. Acta* **266**, 144–162 (2019).

33. F. M. McCubbin *et al*., Magmatic volatiles (H, C, N, F, S, Cl) in the lunar mantle, crust, and regolith: Abundances, distributions, processes, and reservoirs. *Am. Mineral.* **100**, 1668–1707 (2015).
34. R. Kaufmann, A. Long, H. Bentley, S. Davis, Natural chlorine isotope variations. *Nature* **309**, 338–340 (1984).
35. R. Tartèse *et al*., Apatites in lunar KREEP basalts: The missing link to understanding the H isotope systematics of the Moon. *Geology* **42**, 363–366 (2014).
36. R. Tartèse, M. Anand, K. H. Joy, I. A. Franchi, H and Cl isotope systematics of apatite in brecciated lunar meteorites Northwest Africa 4472, Northwest Africa 773, Sayh al Uhaymir 169, and Kalahari 009. *Meteorit. Planet. Sci.* **49**, 2266–2289 (2014).
37. C. Shearer *et al*., Distinct chlorine isotopic reservoirs on Mars. Implications for character, extent and relative timing of crustal interactions with mantle-derived magmas, evolution of the Martian atmosphere, and the building blocks of an early Mars. *Geochim. Cosmochim. Acta* **234**, 24–36 (2018).
38. E. A. Schauble, G. R. Rossman, H. P. Taylor, Theoretical estimates of equilibrium chlorine-isotope fractionations. *Geochim. Cosmochim. Acta* **67**, 3267–3281 (2003).
39. M.-A. Fortin, E. B. Watson, R. Stern, The isotope mass effect on chlorine diffusion in dacite melt, with implications for fractionation during bubble growth. *Earth Planet. Sci. Lett.* **480**, 15–24 (2017).
40. A. El Goresy *et al*., Zinc, lead, chlorine and FeOOH-bearing assemblages in the Apollo 16 sample 66095: Origin by impact of a comet or a carbonaceous chondrite? *Earth Planet. Sci. Lett.* **18**, 411–419 (1973).
41. R. H. Hunter, L. A. Taylor, "Rust and schreibersite in Apollo 16 highland rocks: manifestations of volatile-element mobility" in *Lunar and Planetary Science Conference Proceedings 12*, (Lunar and Planetary Institute, Houston, TX, 1982), pp. 253–259.
42. D. S. McKay, S. J. Wentworth, "Grain surface features of Apollo 17 orange and black glasses" in *Lunar and Planetary Science Conference Proceedings 24*, (Lunar and Planetary Institute, Houston, TX, 1993), pp. 961–962.
43. N. J. Potts *et al*., Characterization of mesostasis regions in lunar basalts: Understanding late-stage melt evolution and its influence on apatite formation. *Meteorit. Planet. Sci.* **51**, 1555–1575 (2016).
44. N. E. Marks, L. E. Borg, C. K. Shearer, W. S. Cassata, Geochronology of an Apollo 16 clast provides evidence for a basin-forming impact 4.3 billion years ago. *J. Geophys. Res. Planets* **124**, 2465–2481 (2019).
45. C. K. Shearer, J. J. Papike, S. B. Simon, N. Shimizu, An ion microprobe study of the intra-crystalline behavior of REE and selected trace elements in pyroxene from mare basalts with different cooling and crystallization histories. *Geochim. Cosmochim. Acta* **53**, 1041–1054 (1989).
46. J. A. Wood, J. Dickey Jr., U. B. Marvin, B. Powell, "Lunar anorthosites and a geophysical model of the moon" in *Geochimica et Cosmochimica Acta Supplement. Proceedings of the Apollo 11 Lunar Science Conference*, A. A. Levinson, Ed. (Pergamon, New York, 1970), Vol. vol. 1, p. 965.
47. G. A. Snyder, L. A. Taylor, C. R. Neal, A chemical model for generating the sources of mare basalts: Combined equilibrium and fractional crystallization of the lunar magmasphere. *Geochim. Cosmochim. Acta* **56**, 3809–3823 (1992).
48. L. T. Elkins-Tanton, T. L. Grove, Water (hydrogen) in the lunar mantle: Results from petrology and magma ocean modeling. *Earth Planet. Sci. Lett.* **307**, 173–179 (2011).
49. W. B. Moore, J. I. Simon, A. A. G. Webb, Heat-pipe planets. *Earth Planet. Sci. Lett.* **474**, 13–19 (2017).
50. C. K. Shearer, J. J. Papike, Early crustal building processes on the moon: Models for the petrogenesis of the magnesian suite. *Geochim. Cosmochim. Acta* **69**, 3445–3461 (2005).
51. C. K. Shearer, S. M. Elardo, N. E. Petro, L. E. Borg, F. M. McCubbin, Origin of the lunar highlands Mg-suite: An integrated petrology, geochemistry, chronology, and remote sensing perspective. *Am. Mineral.* **100**, 294–325 (2015).
52. C. Renggli, P. King, R. Henley, M. Norman, Volcanic gas composition, metal dispersion and deposition during explosive volcanic eruptions on the Moon. *Geochim. Cosmochim. Acta* **206**, 296–311 (2017).
53. C. J. Renggli, S. Klemme, Experimental constraints on metal transport in fumarolic gases. *J. Volcanol. Geotherm. Res.* **400**, 106929 (2020).
54. J. K. Dhaliwal, J. M. Day, F. Moynier, Volatile element loss during planetary magma ocean phases. *Icarus* **300**, 249–260 (2018).
55. H. Vollstaedt, K. Mezger, I. Leya, The selenium isotope composition of lunar rocks: Implications for the formation of the Moon and its volatile loss. *Earth Planet. Sci. Lett.* **542**, 116289 (2020).
56. X. Bu, T. Wang, G. Hall, Determination of halogens in organic compounds by high resolution inductively coupled plasma mass spectrometry (HR-ICP-MS). *J. Anal. At. Spectrom* **18**, 1443–1451 (2003).